

Deformable Organic Nanowire Field-Effect Transistors

Yeongjun Lee, Jin Young Oh, Taeho Roy Kim, Xiaodan Gu, Yeongin Kim, Ging-Ji Nathan Wang, Hung-Chin Wu, Raphael Pfattner, John W. F. To, Toru Katsumata, Donghee Son, Jiheong Kang, James R. Matthews, Weijun Niu, Mingqian He, Robert Sinclair, Yi Cui, Jeffrey B.-H. Tok, Tae-Woo Lee,* and Zhenan Bao*

Deformable electronic devices that are impervious to mechanical influence when mounted on surfaces of dynamically changing soft matters have great potential for next-generation implantable bioelectronic devices. Here, deformable field-effect transistors (FETs) composed of single organic nanowires (NWs) as the semiconductor are presented. The NWs are composed of fused thiophene diketopyrrolopyrrole based polymer semiconductor and high-molecular-weight polyethylene oxide as both the molecular binder and deformability enhancer. The obtained transistors show high field-effect mobility $>8 \text{ cm}^2 \text{ V}^{-1} \text{ s}^{-1}$ with poly(vinylidene fluoride-co-trifluoroethylene) polymer dielectric and can easily be deformed by applied strains (both 100% tensile and compressive strains). The electrical reliability and mechanical durability of the NWs can be significantly enhanced by forming serpentine-like structures of the NWs. Remarkably, the fully deformable NW FETs withstand 3D volume changes ($>1700\%$ and reverting back to original state) of a rubber balloon with constant current output, on the surface of which it is attached. The deformable transistors can robustly operate without noticeable degradation on a mechanically dynamic soft matter surface, e.g., a pulsating balloon (pulse rate: 40 min^{-1} (0.67 Hz) and 40% volume expansion) that mimics a beating heart, which underscores its potential for future biomedical applications.

Development of deformable electronic devices that reshape their original form according to deformation of dynamic soft and living matters with mechanical durability can expand everyday electronic applications to biomedical fields, such as electronic skin, prostheses, and implantable devices for health monitoring.^[1–10] Since a critical parameter for such devices is to be impervious to mechanical influence, ideal devices should thus be easily deformed when mounted on dynamic flexing surfaces while the electronic properties are highly reversible with repeated deformation. Field-effect transistors (FETs) are essential components of deformable electronic devices to reliably control and process electrical signals. However, the development of deformable semiconductors that maintain their electrical properties under mechanical deformation remains rudimentary. Strain-engineered geometric designs such as serpentine pattern, kirigami, and buckling have been widely used to mitigate the effective strain of electronic materials on elastic substrates

Y. Lee

Department of Materials Science and Engineering
Pohang University of Science and Technology (POSTECH)
Pohang, Gyeongbuk 37673, Republic of Korea

Y. Lee, Dr. J. Y. Oh, Dr. X. Gu,^[†] G.-J. N. Wang, Dr. H.-C. Wu,
Dr. R. Pfattner, Dr. J. W. F. To, Dr. T. Katsumata, Dr. D. Son, J. Kang,
Dr. J. B.-H. Tok, Prof. Z. Bao

Department of Chemical Engineering
Stanford University
Stanford, CA 94305, USA
E-mail: zbao@stanford.edu

T. R. Kim, Prof. R. Sinclair, Prof. Y. Cui
Department of Materials Science and Engineering
Stanford University
Stanford, CA 94305, USA

 The ORCID identification number(s) for the author(s) of this article can be found under <https://doi.org/10.1002/adma.201704401>.

^[†]Present address: School of Polymers and High Performance Materials, University of Southern Mississippi, Hattiesburg, MS 39406, USA

DOI: 10.1002/adma.201704401

Dr. X. Gu

Stanford Synchrotron Radiation Lightsource
SLAC National Accelerator Laboratory
Menlo Park, CA 94025, USA

Y. Kim

Department of Electrical Engineering
Stanford University
Stanford, CA 94305, USA

Dr. J. R. Matthews, Dr. W. Niu, Dr. M. He
Corning Incorporated
Corning, NY 14831, USA

Prof. T.-W. Lee

Department of Materials Science and Engineering
Research Institute of Advanced Materials
BK21 PLUS SNU Materials Division for Educating Creative
Global Leaders

Seoul National University
Seoul 08826, Republic of Korea
E-mail: twlees@snu.ac.kr, taewlees@gmail.com

during deformation.^[7–16] For examples, flexible organic thin film FET and organic solar cells can be buckled by depositing the nondeformable thin film on a prestretched elastic substrate.^[7,14] Specifically, Someya et al. used ultrathin substrates to give stable operation within the previously applied strain range, enabling its suitability as a wearable electronic device.^[7] Rogers et al. have recently demonstrated a flexible silicon transistor to record cardiac signals on a heart.^[15] These studies reported innovative improvements in flexible thin-film transistors for wearable and implantable bioelectronics. There is still room for further development of mechanical compatibility of electronic devices with solution-processed deformable semiconducting polymers on mechanically dynamic soft matter surfaces.

Polymer semiconductors with low elastic modulus, high flexibility, and stretchability are promising alternatives for deformable transistor-based bioelectronics. Several strategies have been introduced to increase ductility of conjugated polymer semiconductors to achieve high mechanical compliance: (i) modified side chains or non-conjugated flexible linkers have been incorporated into semiconducting polymer chains, but these approaches inevitably degrade the semiconductor's electrical properties through disruption of molecular packing or conjugated bonding,^[17,18] and (ii) blending semiconducting polymer nanofibril networks into elastomers. The second approach can yield deformable semiconducting films without degrading carrier mobility under strain.^[19] These nanoconfined fibrils in elastomer matrix have been observed to significantly increase the ductility of the conjugated polymer and reduce its elastic modulus.^[19] However, the difficulty in control of the randomly dispersed nanofibrils in the matrix resulted in numerous nanofibril junctions and a long current pathway, thus often degrading its resulting charge carrier transport in the active channel.^[20]

Electrospun organic semiconducting (OSC) nanowires (NWs) are a promising alternative to overcome the above issues.^[21–33] In electrospinning, both high electric field and strong shear force during the jetting process enable the polymer chains to align along the longitudinal direction of OSC NW.^[34–36] This phenomenon is able to facilitate anisotropic charge transport along the NW. The mechanical properties (e.g., elastic modulus, ductility, and toughness) of electrospun OSC NWs can also easily be modified by the polymer formulation.^[37] Applying strain-engineered structures (e.g., serpentine geometry) to the OSC NWs can further enhance mechanical reliability of the organic semiconducting channels in the FETs irrespective of chemical structures of organic semiconductors. Lastly, direct-printed NWs can be aligned on a substrate in nanoscale, hence enabling the elimination of additional tedious lithography-based patterning process.

Here, we present deformable OSC NW FETs using electrospun deformable OSC NWs. We first characterized the electrical and mechanical properties of aligned OSC NWs comprised of a homogeneous mixture of fused thiophene diketopyrrolopyrrole (FT4-DPP)-based semiconducting polymer and polyethylene oxide (PEO) (7:3 w:w). We found that our electrospun OSC NWs with a polymer dielectric poly(vinylidene fluoride-co-trifluoroethylene) (PVDF-TrFE) showed field-effect mobilities as high as $8.45 \text{ cm}^2 \text{ V}^{-1} \text{ s}^{-1}$. In addition, single FT4-DPP:PEO NWs were observed to be highly ductile and flexible, without breaking on the elastic substrate during stretching up to 100% strain along channel length and width directions and even

after release back to their original state. Next, the OSC NWs were further strain engineered by depositing on a prestretched elastic substrate and released to give a serpentine-like geometry. This further improved their mechanical durability during multiple deformations. Since the OSC NWs have good flexibility and ductility, they are able to both conform and adhere to the deformed substrate. Specifically, they are observed not to be delaminated from their mounted dynamic surfaces despite repeated stretching to 100% strain. Encouraged by this observation, we further confirmed the stable operation of our fabricated deformable OSC NW transistors on the surface of a “repeatedly pulsed” balloon to mimic a beating heart. Our data generally indicate that our devices can be highly applicable and promising for implantable biomedical applications.

The OSC NW FETs were fabricated by electrospinning a polymer solution composed of the FT4-DPP-based semiconducting polymer, which is well known for low band gap and high carrier mobility, and low-modulus PEO with high molecular weight (M_w : $400\,000 \text{ g mol}^{-1}$) as a molecular binder and deformability enhancer to help maintain a continuous polymer jet during electrospinning and increase deformability (Figure 1a). Continuous and uniform nanowires were achieved from the weight ratio of 7:3 (FT4-DPP:PEO) which has the highest amount of semiconducting polymer to form percolation of FT4-DPP-polymer domains in our electrospun OSC NW. Single FT4-DPP:PEO NWs with an average diameter of $675 \pm 40 \text{ nm}$ were aligned between grounded parallel electrodes and transferred onto either rigid or elastic substrates (Figure S1a–c, Supporting Information). During electrospinning, both strong electric fields and shear forces are applied to the polymer jet. This can induce alignment of molecular chains along the long axis of the NWs (Figure S1b, Supporting Information).^[34–36] We also obtained polarized optical microscopy images that show high birefringence of NWs arranged diagonally to the polarizer and analyzer indicating that the polymer chains are aligned along the long axis of the NWs (Figure 1a).^[36] We believe that the proper chain alignment contributed to the charge carrier transport through the NWs described below.

An OSC NW FET on an SiO_2/Si substrate (bottom contact and top gate) with a high- κ (10.4) ferroelectric polymer PVDF-TrFE dielectric showed typical current-voltage transfer characteristics and mobility up to $8.45 \text{ cm}^2 \text{ V}^{-1} \text{ s}^{-1}$ (average $7.46 \pm 0.53 \text{ cm}^2 \text{ V}^{-1} \text{ s}^{-1}$) (Figure 1b). The high mobility may be attributed to increased carrier accumulation by the high dielectric constant and polarized dipoles of the ferroelectric polymer dielectric.^[32,38] As a comparison, OSC NW FETs with SiO_2 (300 nm) dielectric (bottom contact and bottom gate) showed a maximum mobility of $1.2 \text{ cm}^2 \text{ V}^{-1} \text{ s}^{-1}$ (average $0.73 \pm 0.16 \text{ cm}^2 \text{ V}^{-1} \text{ s}^{-1}$) which is higher than that of thin-film FETs fabricated under the same condition (pure FT4-DPP-polymer film FET: $9 \times 10^{-2} \text{ cm}^2 \text{ V}^{-1} \text{ s}^{-1}$; FT4-DPP:PEO film FET: $2 \times 10^{-4} \text{ cm}^2 \text{ V}^{-1} \text{ s}^{-1}$) (Figure S2, Supporting Information). The maximum drain current increased linearly as the number of NWs increased (Figure 1c; Figure S3a, Supporting Information). In addition, the OSC NW FETs on the SiO_2/Si substrate showed typical anticlockwise hysteresis in the transfer curve, while transistors with ionic dielectrics typically exhibit clockwise hysteresis. The drain current decay under gate bias stress over time also

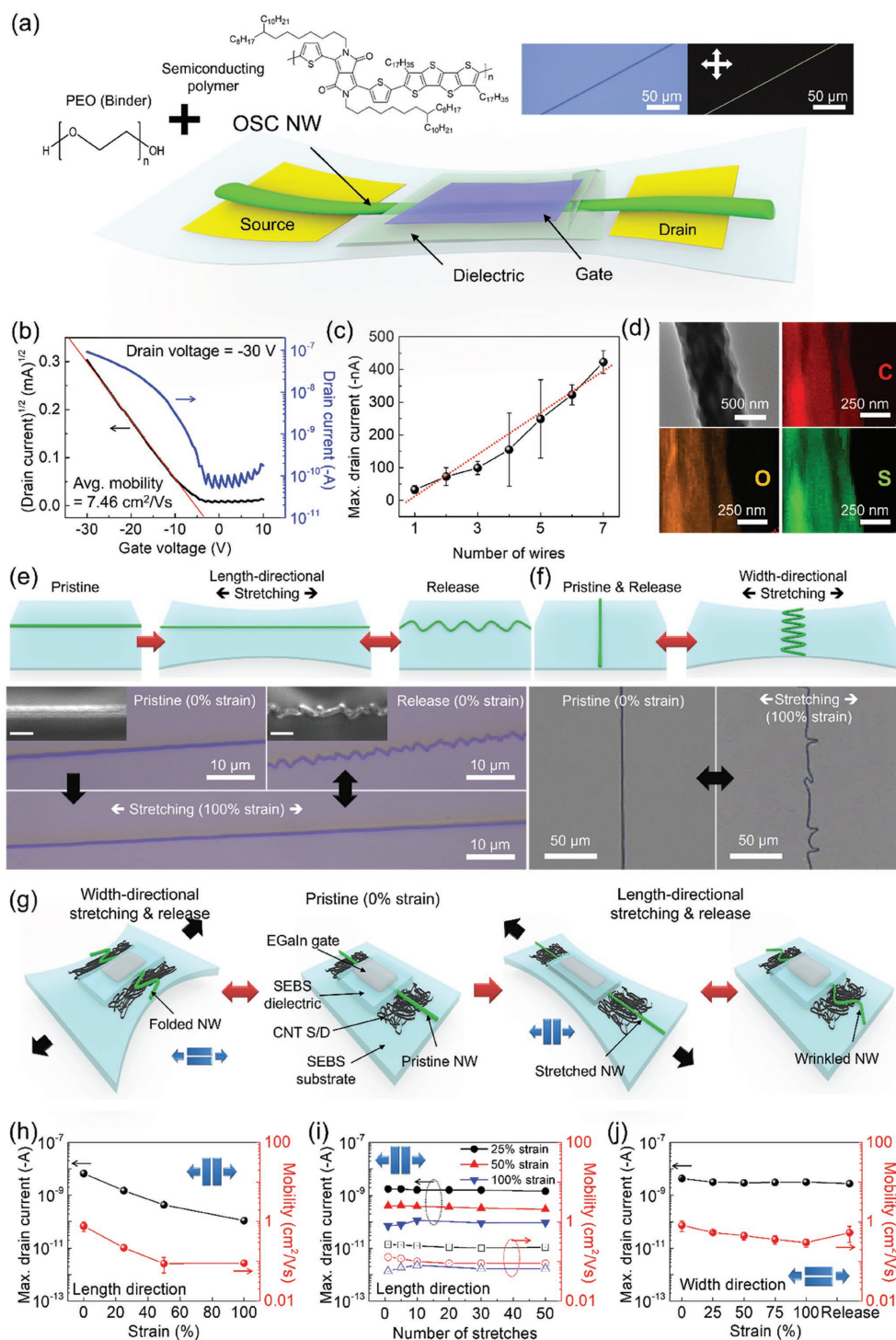


Figure 1. Preparation and characteristics of OSC NW. a) Schematic illustration of OSC NW FET. Chemical structures (upper left) and optical microscope and polarized optical microscope images (upper right) of OSC NW. b) Transfer curves of OSC NW FET with a high- κ (10.4) PVDF-TrFE dielectric (bottom contact and top gate, channel length = 100 μm and width = 675 nm). c) Maximum drain current as a function of the number of OSC NWs (bottom contact and bottom gate, channel length = 150 μm and width = 675 nm). d) Transmission electron microscope image of OSC NW and its elemental mapping using energy-dispersive X-ray spectroscopy. Line profile of OSC NW is presented in Figure S4 (Supporting Information). Schematic and optical microscope images of OSC NWs with e) length-directional stretching (inset: scanning electron microscope images; scale bar: 2 μm) and f) width-directional stretching. g) Schematic illustration of deformable FET with straight OSC NW and SEBS dielectric ($\kappa = 2.1$) with length and width-directional stretching (bottom contact and top gate, channel length = 50 μm and width = 675 nm). Mobility and maximum drain current of deformable FET with straight OSC NW h) under various strains and i) after repeated stretching cycles at 25%, 50%, and 100% strains in the channel length direction. j) Mobility and maximum drain current of deformable FET with straight OSC NW under width-directional strain and after releasing to its original state.

suggests that charge traps are present.^[39,40] These characteristics indicate that the PEO most likely has a negligible double-layer capacitor effect which may also lead to a general overestimation of the mobility value (Figure S3b, Supporting Information).

Next, we observed that the electrospun FT4-DPP:PEO NWs can improve the device's mechanical deformability as compared to the pure FT4-DPP-based semiconducting polymer, most likely by reducing its elastic modulus while increasing toughness.^[37] Moreover, a uniform morphology with a homogeneous chemical composition can further minimize the occurrence and propagation of mechanical defects (Figure 1d; Figure S4, Supporting Information). Single OSC NW placed on a stretchable polydimethylsiloxane or styrene-ethylene-butylene-styrene (SEBS) film was stretched along the length direction up to 100% strain (Figure 1e). The NW was elongated without breaking and interface instability which causes a slip or a delamination of NW from the surface (decreased diameter \approx 280 nm) (Figure 1e; Figure S5, Supporting Information). The FT4-DPP:PEO NWs were able to accommodate much larger mechanical deformations than the pure FT4-DPP-polymer and FT4-DPP:PEO films that exhibited cracks and defects even at a small strain (<20%) (Figure S6, Supporting Information).

The elastic modulus of FT4-DPP:PEO NWs and pure FT4-DPP-polymer and FT4-DPP:PEO films were analyzed using both the peak-force quantitative nanomechanical method and the buckling method (Figures S7 and S8, Supporting Information).^[17-19,41-43] The FT4-DPP:PEO NW and film showed similar measured elastic moduli of 303 and 496 MPa, respectively, which are lower than that of the pure FT4-DPP-polymer film (960 MPa) (Figure S8, Supporting Information). The low measured elastic modulus (230 MPa) of PEO which was ductile and developed crazing but no severe cracks at 100% strain (Figure S6e, Supporting Information)^[44] contributed to lower elastic moduli of the blend NWs and films.^[37] The FT4-DPP:PEO films developed smaller cracks than the pure FT4-DPP-polymer film at 20% strain, but had a lower toughness than the NWs (which have alignment of the polymer chains and accommodate much larger strain) (Figure S6b, Supporting Information).^[37] The elongated straight NWs became wrinkled on the rubbery substrate during strain release (Figure 1e). Additional repeated stretching cycles merely unfolded the wrinkled structure, so the deformed NWs did not break. Meanwhile, during width-directional stretching up to 100% strain, the pristine NWs were folded in parts by compressive strain, but because of the high flexibility of the NWs, they are able to recover their original shape without significant plastic deformation after strain release (Figure 1f).

To evaluate the intrinsic electrical properties of the OSC NWs during stretching, deformable FETs were fabricated with straight OSC NWs. The process is as follows: carbon nanotube source and drain (S/D) electrodes were first transferred onto the SEBS elastomer substrate. The straight OSC NW was then transferred onto the S/D electrodes. Nonionic SEBS dielectric (2 μ m, κ = 2.1)^[45] and the eutectic gallium-indium (EGaIn) gate electrode were subsequently transferred onto the OSC NW (Figure 1g; Figure S9, Supporting Information). At 0% strain, the FETs were measured with an average mobility = 0.78 ± 0.21 cm² V⁻¹ s⁻¹ and an average maximum drain

current = -6.7 ± 1.88 nA at gate and drain voltage = -100 V. As the tensile strain was increased to 100% (channel length direction), the deformable transistor continued to function properly; however, its mobility decreased to below 0.1 cm² V⁻¹ s⁻¹ due to plastic deformation (Figure 1h, Supporting Information). Nonetheless, the mobility was maintained at above 0.08 cm² V⁻¹ s⁻¹, even when the strain was released. The elongated NWs showed high electrical stabilities during multiple stretching cycles (50 times) at 25%, 50%, and 100% strains (Figure 1i; Figure S10a-e, Supporting Information). Both mobility and drain current were observed to vary by <20% during cyclic stretching because the wrinkled OSC NWs can efficiently release the applied strain by straightening without further elongation of the NWs. In contrast, along the perpendicular direction to stretching, both mobility and drain current were almost maintained even up to 100% strain. We reasoned that this is because the OSC NWs were not actually stretched, but rather they were folded by compressive strain to the longitudinal direction of OSC NWs (Figure 1f; Figure S11, Supporting Information). The initial mobility of 0.82 ± 0.25 cm² V⁻¹ s⁻¹ and drain current of -4.37 ± 0.29 nA became 0.3 ± 0.07 cm² V⁻¹ s⁻¹ and -3.2 nA at 100% strain, and 0.54 ± 0.23 cm² V⁻¹ s⁻¹ and -2.8 nA after being released from 100% strain (Figure 1j; Figure S10f, Supporting Information).

To further investigate the decrease in electrical properties of OSC NWs during elongation under strain, the crystalline structures of NWs were measured using grazing incidence X-ray diffraction (GIXD), both before and after NW length-directional stretching. To separately investigate the FT4-DPP semiconducting polymer and the insulating polymer PEO in the NWs, the PEO of each pristine and stretched NW was selectively etched by methanol washing because the PEO polymer is also semicrystalline which diffracts X-rays. PEO removal was confirmed by Fourier-transform infrared spectroscopy, which indicated a decrease in the absorbance bands at \approx 1100 cm⁻¹, attributed to C-O-C stretching of PEO (Figure S12a, Supporting Information).^[33] The NWs without PEO still showed uniform continuous structures with a reduced average diameter of 613 ± 39 nm and maintained the highly aligned FT4-DPP-polymer chains (Figure 2a, upper; Figure S12b-e, Supporting Information). The 2D image and 1D out-of-plane profiles of GIXD all indicated that the peaks of the (*h*00) lamellae crystal plane differed slightly before and after stretching (Figure 2b; Figure S12f, Supporting Information). Specifically, the periodic distance (*d*-spacing) between planes of the OSC NWs decreased from 2.69 nm (before stretching) to 2.62 nm (after stretching to 100% strain) due to the thinning of the NWs which might compress the unit cell in the lamella direction. A clear (010) peak that corresponds to the strong intermolecular π - π interaction of aligned FT4-DPP-polymer domains in the NWs was significantly decreased, and the π - π stacking distance also increased from 3.71 Å (before stretching) to 3.76 Å (after stretching to 100% strain).^[46] Both above factors may have impeded electrical charge transport in the stretched NWs (Figure 2b; Table S1, Supporting Information). In contrast, PEO-etched NWs were broken at relatively small strains (25%) due to the removal of PEO that enhanced the mechanical ductility of the OSC NWs (Figure 2a, middle and lower).

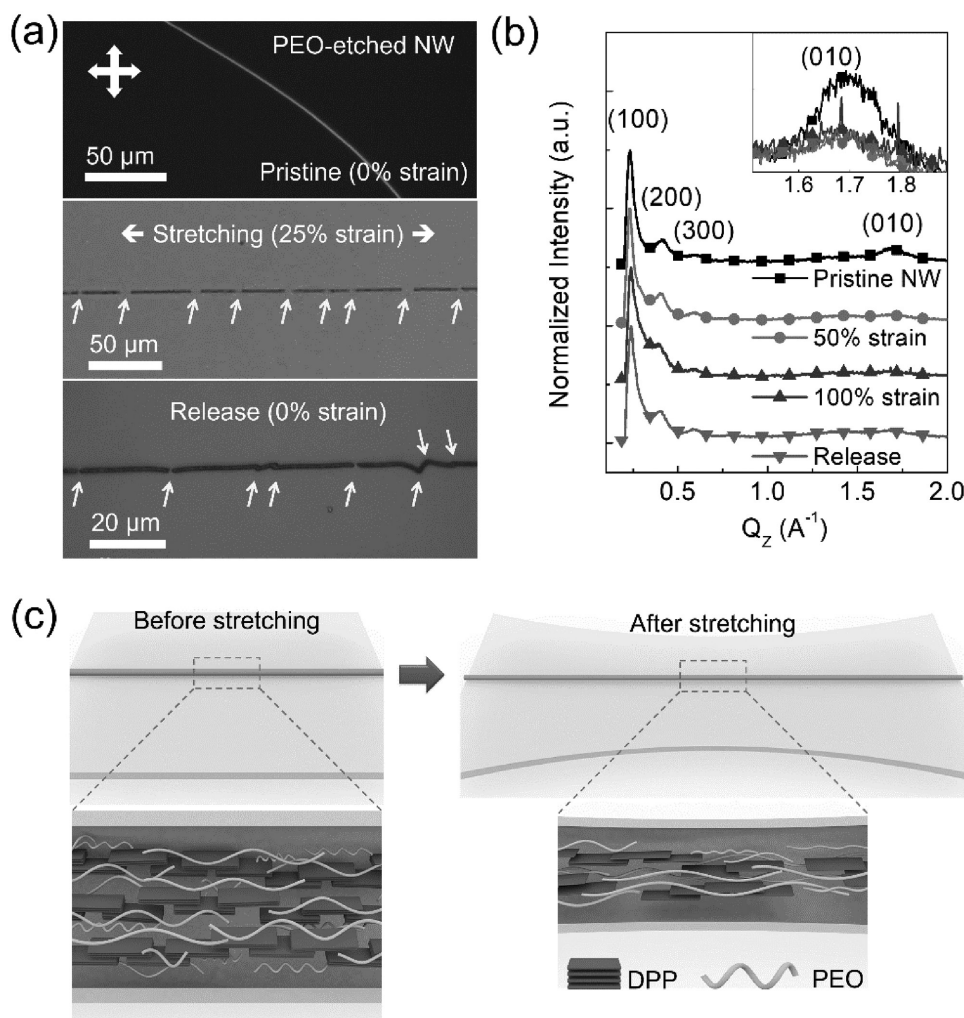


Figure 2. Morphological analysis of OSC NWs. a) Polarized optical microscope (upper) and optical microscope (middle and lower) images of PEO-etched NW with 0% (upper) and 25% (middle) strains in length direction and after release (lower). Arrows indicate broken regions. b) 1D out-of-plane profiles of GIXD analysis of PEO-etched NW stretched with 0%, 50%, and 100% strain in length direction and after release. c) Schematic illustration of the morphological changes in OSC NW during the stretching process.

In the FT4-DPP:PEO NWs (Figure 2c), FT4-DPP-polymer and PEO chains are preferentially aligned in the longitudinal direction of the NWs, as determined by birefringence using a polarized optical microscope.^[36] During stretching, high- M_w PEO maintains a continuous structure to provide support to the OSC NWs, while the FT4-DPP crystalline lamellar structures might unfold and the π - π distance increases slightly.^[46] The π - π interaction consequently weakens, as supported by the reduced intensity of the (010) peak. During stretching along the width direction of the NWs at 100% strain, the PEO-etched OSC NWs were folded by compressive strain along the long axis of the NWs and were able to mostly recover to their pristine shape (similar to the OSC NWs without PEO etching; Figure S12g,h, Supporting Information).

To increase the mechanical durability of deformable FETs, the OSC NW is further strain engineered to form a serpentine-like structure that can prevent degradation of the electrical properties during plastic elongation (Figure 3a). The serpentine structure was formed by prestretching an elastic

substrate at prestrains of 25%, 50%, 75%, and 100%, respectively (Figure S13, Supporting Information). The serpentine OSC NW, as fabricated on the 100% prestrained substrate, was observed to be straight and continuous without elongation even when strained to 100% (Figure 3a). The maximum mobility of deformable FET with a serpentine OSC NW ($1.15 \text{ cm}^2 \text{ V}^{-1} \text{ s}^{-1}$) was similar to that of the device with a straight OSC NW ($1.1 \text{ cm}^2 \text{ V}^{-1} \text{ s}^{-1}$), which indicates that the compressive strain to form the serpentine structure of OSC NW did not affect the electrical property of the OSC NW. FETs with serpentine OSC NWs also showed stable mobility and drain current when subjected to stretching up to 100% strain in both channel length and width directions without significant electrical loss (Figure 3b-d; Figure S14, Supporting Information). At 100% strain along the channel length direction, our devices displayed an average mobility = $0.35 \pm 0.06 \text{ cm}^2 \text{ V}^{-1} \text{ s}^{-1}$ and maximum drain current = $-1.29 \pm 0.28 \text{ nA}$, which is on the same order of magnitude as the value before stretching (average mobility = $1.05 \pm 0.09 \text{ cm}^2 \text{ V}^{-1} \text{ s}^{-1}$; maximum drain

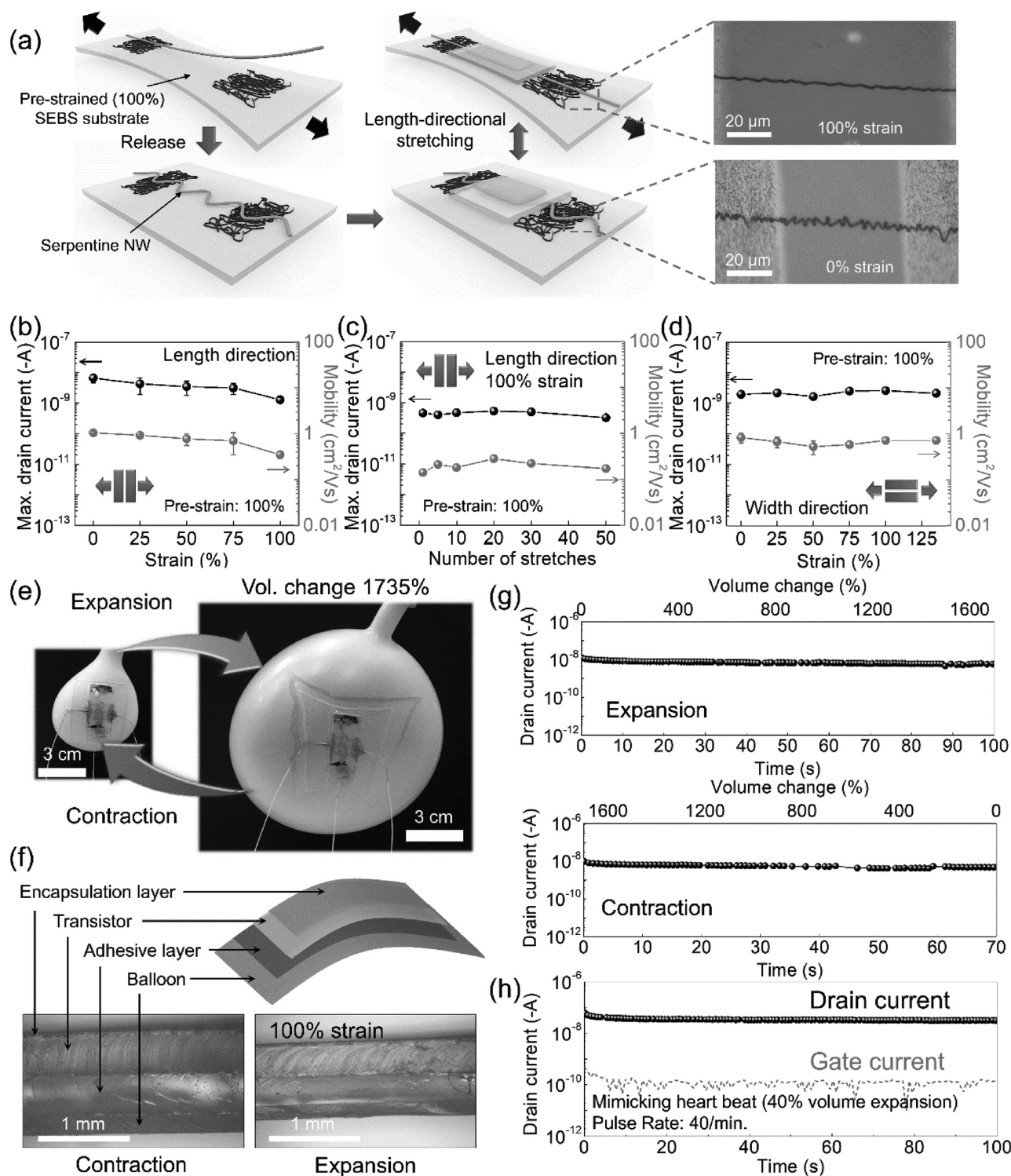


Figure 3. Deformable FET with serpentine OSC NW. a) Schematic illustration of the fabrication process of deformable FET with serpentine OSC NW (prestrain: 100%) and SEBS dielectric ($\kappa = 2.1$) (bottom contact and top gate, channel length = 100 μm and width = 675 nm). Optical microscope images show the serpentine OSC NW before and after stretching. Mobility and maximum drain current of deformable FET with serpentine OSC NW (prestrain: 100%) b) under various strains and c) after repeated stretching cycles at 100% strain in channel length direction. d) Mobility and maximum drain current of deformable FET with serpentine OSC NW (prestrain: 100%) under width-directional strain and after strain release. e) Digital images of a deformable FET with serpentine OSC NW mounted on the dynamic surface of a pulsating balloon that mimics a beating heart. f) Specific layout and cross-sectional optical microscope images of device attached on the balloon. g) Drain current of the deformable FET on the balloon during >1700% volume expansion (upper) and contraction to original shape (lower). h) Drain current and gate current of the deformable FET on a repeatedly pulsed balloon with $\approx 40\%$ volume change at a pulse rate of 40 min^{-1} (0.67 Hz).

current = -6.65 ± 2.05 nA) (Figure 3b; Figure S14a, Supporting Information). Upon stretching at 100% strain perpendicular to the long axis of the NWs, mobility and maximum drain current of the devices changed from 0.83 ± 0.2 cm² V⁻¹ s⁻¹ and -1.96 ± 0.44 nA to 0.65 ± 0.07 cm² V⁻¹ s⁻¹ and -2.56 ± 0.05 nA, respectively (Figure 3d; Figure S14c, Supporting Information). In addition, the electrical property of the device was unaffected even after repeated stretching cycles (50 times) to 100% strain in both directions (Figure 3c; Figure S14b,d, Supporting Information).

To demonstrate the feasibility of our prepared OSC NW-based stretchable FETs for deformable electronics, it was necessary to demonstrate that our deformable transistor would also function robustly when mounted on a dynamically soft material. To test this possibility, we first attach our fabricated deformable FET with a serpentine OSC NW (on 500 μm thick SEBS substrate) onto the surface of a 300 μm thick latex balloon (Aldrich) that was able to undergo 3D volume expansion and contraction (Figure 3e). The deformable FET was stably fixed with a 500 μm thick elastic adhesive tape (3M VHB) and encapsulated with a thin (<100 μm) polyurethane adhesive film (3M Tegaderm) (Figure 3f). The device was then expanded and contracted when suitably mounted on the balloon surface without observable mechanical delamination (Figure 3f). We observed that the derived drain current (gate voltage = drain voltage = -60 V) remained stable while the balloon's volume expanded to >1700% and returning back to its original shape, i.e., 0% (Figure 3g). The device area was extended to 130% during the volume expansion of the balloon to 1700% because of the elastic modulus difference between the SEBS substrate (1 MPa)^[19] and the latex balloon (the initial elastic modulus of 680 kPa decreased as strain increased).^[47] The drain current of a FET with a straight OSC NW dropped significantly with the volume expansion of the balloon to 900% (Figure S15, Supporting Information), implying that the 3D strain on the OSC NW is too harsh a condition to maintain the electrical properties of the device. In the future, the modulus of deformable FETs will be further optimized by material design to match with the moduli of human tissues (<100 kPa)^[48] for applications in bio-implantable systems. Next, we tested our device on a balloon that was repeatedly pulsed (average volume expansion: 40%; pulse rate: 40 min⁻¹ (0.67 Hz)) to mimic a beating heart. The drain current of the device displayed negligible changes (Figure 3h; Movie S1, Supporting Information), which underlined the robustness of the device. Thus, our deformable devices are highly applicable to the dynamic 3D surfaces, e.g., human organ, that are perpetually undergoing mechanical expansion and contraction. Moving forward, these deformable FETs based on OSC NWs may be applied in biomedical electronics for sensing and signal processing circuits.

In summary, we report here deformable FETs based on electrospun OSC NWs. The homogeneously blended OSC NWs, comprised of an FT4-DPP and PEO polymer blend, are observed to be highly ductile and deformable. When these fully deformable devices were subjected to both 100% tensile strain and release, we observed that their conducting pathways are preserved through the OSC NWs. However, the applied tensile strains nonetheless caused plastic deformation of the NW, which resulted in minor reduction in its electrical transport properties. On the other hand, the stretched OSC NWs generated wrinkled

structures upon strain release and, importantly, showed no further degradation of electrical properties upon subsequent restraining, within the previously applied strain range. Strain-engineered serpentine structures were subsequently prepared using our OSC NWs to prevent plastic deformation. In addition, the FETs based on serpentine OSC NWs were observed to be stable against further deformation and are therefore able to preserve their electrical properties without degradation even after both 100% tensile strain and release. Lastly, our deformable FET can stably function when mounted on the surface of a soft dynamic balloon, in which its volume expansion can reach more than 1700%. We demonstrated that electrical measurements can be robustly performed on a mechanically dynamic soft matter surface. Furthermore, this pulsating balloon mimics a beating heart, and hence suggests our OSC NW-based FETs may be compatible with use in implantable medical devices. Taken together, our described deformable FETs based on OSC NWs greatly advance deformable electronics to equip next-generation biological and soft electronic applications.

Supporting Information

Supporting Information is available from the Wiley Online Library or from the author.

Acknowledgements

Y.L. and J.Y.O. contributed equally to this work. This work was partly supported by the Center for Advanced Soft-Electronics funded by the Ministry of Science, ICT and Future Planning as Global Frontier Project (2013M3A6A5073175) and the National Research Foundation of Korea (NRF) grant funded by the Korea government (Ministry of Science, ICT and Future Planning) (NRF-2016R1A3B1908431). X.G. acknowledges support from the Bridging Research Interactions through the collaborative Development Grants in Energy (BRIDGE) program under the SunShot initiative of the Department of Energy program (Contract No. DE-FOA-0000654-1588). GIXD were carried out at the Stanford Synchrotron Radiation Laboratory, a national user facility operated by Stanford University on behalf of the U.S. Department of Energy, Office of Basic Energy Sciences (Contract No. DE-AC02-76SF00515). This work was also partly supported by Samsung Electronics.

Conflict of Interest

The authors declare no conflict of interest.

Keywords

biomedical electronics, deformable electronics, nanowire electronics, nanowire transistors, stretchable transistors

Received: August 4, 2017
Revised: September 27, 2017
Published online: January 8, 2018

[1] M. L. Hammock, A. Chortos, B. C.-K. Tee, J. B.-H. Tok, Z. Bao, *Adv. Mater.* **2013**, *25*, 5997.

[2] T. Someya, Z. Bao, G. G. Malliaras, *Nature* **2016**, *540*, 379.

- [3] A. Chortos, J. Liu, Z. Bao, *Nat. Mater.* **2016**, *15*, 937.
- [4] S. Lee, A. Reuveny, J. Reeder, S. Lee, H. Jin, Q. Liu, T. Yokota, T. Sekitani, T. Isoyama, Y. Abe, Z. Suo, T. Someya, *Nat. Nanotechnol.* **2016**, *11*, 472.
- [5] J. Y. Oh, S. Kim, H.-K. Baik, U. Jeong, *Adv. Mater.* **2016**, *28*, 4455.
- [6] T. Sekitani, T. Yokota, K. Kuribara, M. Kaltenbrunner, T. Fukushima, Y. Inoue, M. Sekino, T. Isoyama, Y. Abe, H. Onodera, T. Someya, *Nat. Commun.* **2016**, *7*, 11425.
- [7] M. Kaltenbrunner, T. Sekitani, J. Reeder, T. Yokota, K. Kuribara, T. Tokuhara, M. Drack, R. Schwödauer, I. Graz, S. Bauer-Gogonea, S. Bauer, T. Someya, *Nature* **2013**, *499*, 458.
- [8] J. A. Rogers, T. Someya, Y. Huang, *Science* **2010**, *327*, 1603.
- [9] D.-H. Kim, N. Lu, R. Ma, Y.-S. Kim, R.-H. Kim, S. Wang, J. Wu, S. M. Won, H. Tao, A. Islam, K. J. Yu, T.-i. Kim, R. Chowdhury, M. Ying, L. Xu, M. Li, H.-J. Chung, H. Keum, M. McCormick, P. Liu, Y.-W. Zhang, F. G. Omenetto, Y. Huang, T. Coleman, J. A. Rogers, *Science* **2011**, *333*, 838.
- [10] D.-H. Kim, N. Lu, R. Ghaffari, Y.-S. Kim, S. P. Lee, L. Xu, J. Wu, R.-H. Kim, J. Song, Z. Liu, J. Viventi, B. de Graff, B. Elolampi, M. Mansour, M. J. Slepian, S. Hwang, J. D. Moss, S.-M. Won, Y. Huang, B. Litt, J. A. Rogers, *Nat. Mater.* **2011**, *10*, 316.
- [11] T. C. Shyu, P. F. Damasceno, P. M. Dodd, A. Lamoureux, L. Xu, M. Shlian, M. Shtein, S. C. Glotzer, N. A. Kotov, *Nat. Mater.* **2015**, *14*, 785.
- [12] M. K. Bles, A. W. Barnard, P. A. Rose, S. P. Roberts, K. L. McGill, P. Y. Huang, A. R. Ruyack, J. W. Kevek, B. Kobrin, D. A. Muller, P. L. McEuen, *Nature* **2015**, *524*, 204.
- [13] D.-Y. Khang, H. Jiang, Y. Huang, J. A. Rogers, *Science* **2006**, *311*, 208.
- [14] D. J. Lipomi, B. C.-K. Tee, M. Vosgueritchian, Z. Bao, *Adv. Mater.* **2011**, *23*, 1771.
- [15] H. Fang, K. J. Yu, C. Gloschat, Z. Yang, E. Song, C.-H. Chiang, J. Zhao, S. M. Won, S. Xu, M. Trumpis, Y. Zhong, S. W. Han, Y. Xue, D. Xu, S. W. Choi, G. Cauwenberghs, M. Kay, Y. Huang, J. Viventi, I. R. Efimov, J. A. Rogers, *Nat. Biomed. Eng.* **2017**, *1*, 38.
- [16] T. Yokota, P. Zalar, M. Kaltenbrunner, H. Jinno, N. Matsuhisa, H. Kitano, Y. Tachibana, W. Yukita, M. Koizumi, T. Someya, *Sci. Adv.* **2016**, *2*, e1501856.
- [17] J. Y. Oh, S. Rondeau-Gagné, Y.-C. Chiu, A. Chortos, F. Lissel, G.-J. N. Wang, B. C. Schroeder, T. Kurosawa, J. Lopez, T. Katsumata, J. Xu, C. Zhu, X. Gu, W.-G. Bae, Y. Kim, L. Jin, J. W. Chung, J. B.-H. Tok, Z. Bao, *Nature* **2016**, *539*, 411.
- [18] G.-J. N. Wang, L. Shaw, J. Xu, T. Kurosawa, B. C. Schroeder, J. Y. Oh, S. J. Benight, Z. Bao, *Adv. Funct. Mater.* **2016**, *26*, 7254.
- [19] J. Xu, S. Wang, G.-J. N. Wang, C. Zhu, S. Luo, L. Jin, X. Gu, S. Chen, V. R. Feig, J. W. F. To, S. Rondeau-Gagné, J. Park, B. C. Schroeder, C. Lu, J. Y. Oh, Y. Wang, Y.-H. Kim, H. Yan, R. Sinclair, D. Zhou, G. Xue, B. Murmann, C. Linder, W. Cai, J. B.-H. Tok, J. W. Chung, Z. Bao, *Science* **2017**, *355*, 59.
- [20] M. Shin, J. Y. Oh, K.-E. Byun, Y.-J. Lee, B. Kim, H.-K. Baik, J.-J. Park, U. Jeong, *Adv. Mater.* **2015**, *27*, 1255.
- [21] A. Manuelli, L. Persano, D. Pisignano, *Org. Electron.* **2014**, *15*, 1056.
- [22] M. Y. Lee, J. Hong, E. K. Lee, H. Yu, H. Kim, J. U. Lee, W. Lee, J. H. Oh, *Adv. Funct. Mater.* **2016**, *26*, 1445.
- [23] M. Shin, J. H. Song, G.-H. Lim, B. Lim, J.-J. Park, U. Jeong, *Adv. Mater.* **2014**, *26*, 3706.
- [24] S. W. Lee, H. J. Lee, J. H. Choi, W. G. Koh, J. M. Myoung, J. H. Hur, J. J. Park, J. H. Cho, U. Jeong, *Nano Lett.* **2010**, *10*, 347.
- [25] S. Lee, G. D. Moon, U. Jeong, *J. Mater. Chem.* **2009**, *19*, 743.
- [26] J.-Y. Chen, H.-C. Wu, Y.-C. Chiu, C.-J. Lin, S.-H. Tung, W.-C. Chen, *Adv. Electron. Mater.* **2015**, *1*, 1400028.
- [27] C.-C. Chou, H.-C. Wu, C.-J. Lin, E. Ghelichkhani, W.-C. Chen, *Macromol. Chem. Phys.* **2013**, *214*, 751.
- [28] P.-Z. Jian, Y.-C. Chiu, H.-S. Sun, T.-Y. Chen, W.-C. Chen, S.-H. Tung, *ACS Appl. Mater. Interfaces* **2014**, *6*, 5506.
- [29] S.-Y. Min, T.-S. Kim, Y. Lee, H. Cho, W. Xu, T.-W. Lee, *Small* **2015**, *11*, 45.
- [30] H. Cho, S.-Y. Min, T.-W. Lee, *Macromol. Mater. Eng.* **2013**, *298*, 475.
- [31] S.-Y. Min, T.-S. Kim, B. J. Kim, H. Cho, Y.-Y. Noh, H. Yang, J. H. Cho, T.-W. Lee, *Nat. Commun.* **2013**, *4*, 1773.
- [32] S. K. Hwang, S.-Y. Min, I. Bae, S. M. Cho, K. L. Kim, T.-W. Lee, C. Park, *Small* **2014**, *10*, 1976.
- [33] E. V. Canesi, A. Luzio, B. Saglio, A. Bianco, M. Caironi, C. Bertarelli, *ACS Macro Lett.* **2012**, *1*, 366.
- [34] T. Han, A. L. Yarin, D. H. Reneker, *Polymer* **2008**, *49*, 1651.
- [35] M. V. Kakade, S. Givens, K. Gardner, K. H. Lee, D. B. Chase, J. F. Rabolt, *J. Am. Chem. Soc.* **2007**, *129*, 2777.
- [36] Y.-J. Kim, D.-Y. Kim, J.-H. Lee, C. Nah, J. H. Lee, M.-H. Lee, H. Y. Kim, S.-W. Kuo, S. Shin, K.-U. Jeong, *J. Mater. Chem.* **2012**, *22*, 13477.
- [37] R. L. Andersson, V. Ström, U. W. Gedde, P. E. Mallon, M. S. Hedenqvist, R. T. Olsson, *Sci. Rep.* **2014**, *4*, 6335.
- [38] D. Khim, Y. Xu, K.-J. Baeg, M. Kang, W.-T. Park, S.-H. Lee, I.-B. Kim, J. Kim, D.-Y. Kim, C. Liu, Y.-Y. Noh, *Adv. Mater.* **2016**, *28*, 518.
- [39] S. Vasimalla, N. V. V. Subbarao, P. K. Iyer, *J. Mater. Chem. C* **2016**, *4*, 7102.
- [40] C. Wang, W.-Y. Lee, D. Kong, R. Pfattner, G. Schweicher, R. Nakajima, C. Lu, J. Mei, T. H. Lee, H.-C. Wu, J. Lopez, Y. Diao, X. Gu, S. Himmelberger, W. Niu, J. R. Matthews, M. He, A. Salles, Y. Nishi, Z. Bao, *Sci. Rep.* **2015**, *5*, 17849.
- [41] J. Adamcik, A. Berquand, R. Mezzenga, *Appl. Phys. Lett.* **2011**, *98*, 193701.
- [42] J. Adamcik, C. Lara, I. Usov, J. S. Jeong, F. S. Ruggieri, G. Dietler, H. A. Lashuel, I. W. Hamley, R. Mezzenga, *Nanoscale* **2012**, *4*, 4426.
- [43] C. M. Stafford, C. Harrison, K. L. Beers, A. Karim, E. J. Amis, M. R. Vanlandingham, H.-C. Kim, W. Volksen, R. D. Miller, E. E. Simonyi, *Nat. Mater.* **2004**, *3*, 545.
- [44] X. Xu, F. Liu, L. Jiang, J. Y. Zhu, D. Haagenson, D. P. Wiesenborn, *ACS Appl. Mater. Interfaces* **2013**, *5*, 2999.
- [45] D. Kong, R. Pfattner, A. Chortos, C. Lu, A. C. Hinckley, C. Wang, W.-Y. Lee, J. W. Chung, Z. Bao, *Adv. Funct. Mater.* **2016**, *26*, 4680.
- [46] J. Zhou, E. Q. Li, R. Li, X. Xu, I. A. Ventura, A. Moussawi, D. H. Anjum, M. N. Hedhili, D.-M. Smilgies, G. Lubineau, S. T. Thoroddsen, *J. Mater. Chem. C* **2015**, *3*, 2528.
- [47] M. J. Silva, A. O. Sanches, L. F. Malmonge, J. A. Malmonge, *Mater. Res.* **2014**, *17*, 59.
- [48] X. Liang, S. A. Boppart, *IEEE Trans. Biomed. Eng.* **2010**, *57*, 953.